



3D Modeling and Tectonic Interpretation of the Erzincan Basin (Turkey) using Potential Field Data

Ömer L. Aydın¹, Özcan Bektaş², Aydın Büyüksaraç³, Hüseyin Yılmaz²

¹Erzurum Metropolitan Municipality, TR-25100, Erzurum-Turkey

²Cumhuriyet University, Faculty of Engineering, TR-58100, Sivas-Turkey

³Bitlis Eren University, Faculty of Engineering and Architecture, TR-13000 Bitlis-Turkey

* Corresponding author: ozcanbektas@gmail.com

ABSTRACT

Erzincan Basin was investigated using gravity data within the scope of this study. It is also aimed to reveal the discontinuities in the work area as well as the buried discontinuities. Boundary determination filters and analysis of the structure of the data and its connection are revealed and clear information is obtained. Gravity anomalies were applied with an upward continuation method for 0.25, 0.50, 0.75 and 1 km levels. Total Horizontal Derivative (THD) filter, Analytical Signal (AS) filter, Tilt Angle Derivative (Tilt) filter, Total Horizontal Derivative (THDR) filter, Theta Angle Derivative (Cos θ) filter, Hyperbolic Tilt Angle Derivative (HTAD) were applied to upward continued data. The discontinuities in the region and the boundaries of the geological structure were revealed. Tilt and Theta Angle derivatives yield the best results from the applied derivative based filters. The obtained data were compared with the existing surface geology and the compatibility between the formations was checked. New discontinuities were found in addition to the discontinuities determined from surface observations in the light of the obtained results. Erzincan Basin was modeled in three dimensions using gravity data of the study area. As a result of modeling, Erzincan Basin has been determined to have an average thickness of 7 km.

Keywords: Erzincan Basin, Gravity data, 3D modeling, Derivative based filters.

Modelación 3D e interpretación tectónica en la cuenca Erzincan (Turquía) a través de Información de Campo Potencial

RESUMEN

El objeto de este estudio fue investigar la cuenca Erzincan a través de información gravitacional. También está enfocado en revelar las discontinuidades en el área de estudio así como las discontinuidades enterradas. Se exponen los filtros de determinación de límites y los análisis de la estructura de la información para obtener información clara. El método de continuación hacia arriba se aplicó en las anomalías gravitacionales en niveles de 0.25, 0.50, 0.75 y 1 km. A la información continuada hacia arriba se le aplicaron los filtros Total Horizontal de Derivadas (THD), Señal Analítica (AS), Ángulo Inclinado de Derivadas (Tilt), Ángulo Theta de Derivadas (Cos θ), y Ángulo Inclinado Hiperbólico de Derivadas (HTAD). Este proceso permitió revelar las discontinuidades en la región y los límites de la estructura geológica. Las derivadas de Ángulo Inclinado y Ángulo Theta produjeron los mejores resultados en cuanto a las derivadas aplicadas con base en filtros. La información obtenida se comparó con estudios de superficie geológica y se revisó la compatibilidad entre las formaciones. Se encontraron nuevas discontinuidades adicionales a las discontinuidades determinadas en las observaciones de superficie a la luz de los resultados obtenidos. La cuenca Erzincan se modeló en tres dimensiones con información gravitacional en el área de estudio. Como resultado de la modelación, se determinó que la cuenca Erzincan tiene un promedio de profundidad de 7 kms.

Palabras clave: Cuenca Erzincan; información gravitacional; modelación 3D; derivadas basadas en filtros.

Record

Manuscript received: 23/03/2018

Accepted for publication: 24/08/2018

How to cite item

Aydın, O. L., Bektaş, O., Büyüksaraç, A., & Yılmaz, H. (2019). 3D Modeling and Tectonic Interpretation of the Erzincan Basin (Turkey) using Potential Field Data. *Earth Sciences Research Journal*, 23(1), 57-66.

DOI: <https://doi.org/10.15446/esrj.v23n1.71090>

Introduction

The Erzincan Basin is the largest sedimentary basin on the North Anatolian Fault Zone (NAFZ). Many earthquakes have ruptured the NAFZ within the Erzincan Basin and caused major damage. In the last century, there were two of them ($M_s = 8.0$ in 1939 and $M_s = 6.8$ in 1992) (Barka and Kadinsky-Cade, 1988; Fuenzalida et al., 1997). The 1992 event claimed 541 lives (Barka and Eyidogan, 1993) and had a peak ground acceleration of 0.5 g, and the Mercalli intensity was estimated as IX (Erdik et al., 1992; Gundogdu et al., 1992). Pınar et al. (1994) pointed out the 1992 earthquake have occurred at the eastern end of 1939 earthquake in 350 m long rupture zone. The amount of amplification depends on the thickness and geometry of the basin. Geophysical constraints can be used to image basin depth and causative discontinuities. The seismic hazard in Erzincan from future earthquakes on the NAFZ is significant because the unconsolidated sedimentary basin can amplify the ground motion during an earthquake (Kaypak, 2008).

The analysis of Bayrak et al. (2005) suggested that earthquakes up to magnitude 7.5 could be expected in the Erzincan Basin, and Hartleb et al. (2006) estimated the earthquake recurrence interval as 210–700 years from paleoseismic studies.

The strength of ground motion depends primarily on the thickness of sediments in the basin, with the largest amplification occurring in the deepest parts of the Electronic supplementary material. The thickness and shape of the sedimentary basin are important parameters to predict the amplification of the ground motion. Furthermore, the depth of the basin is an important parameter for improving 3D earthquake relocation (Aktar et al., 2004). Several seismic tomography experiments have attempted to map the thickness of the Erzincan Basin. Some of these studies used the 1992 aftershocks and reported the thickness of unconsolidated sediments as 2–4 km. They determined that the boundary between the upper sedimentary layer and basement was at a depth of 6–12 km. (Aktar et al., 2004; Gokalp, 2007; Kaypak, 2008).

The region's evolution was won by the closure of Paleo-Tethys and its emplaced Karakaya Ocean before Liassic, and the different arms of the Neo-Tethyan Ocean at the end of Cretaceous. After the Neo-Tethys closure, the area became largely land and covered with shallow seas in Eocene and Lower Miocene. Both marine environments, however, did not have a long life due to the thrust structure and rise of the zone with a north-south compression. In the neo-tectonic period beginning from the end of the Lower Miocene, the escape tectonics of the region were effective and lateral strike-slip faults with different strike and extension were developed (Barka and Gulen, 1989).

Hartleb et al. (2006) conducted paleosismological studies on Çukurçimen on the NAFZ in the north-western part of the Erzincan Basin. They say that there are at least six and possibly seven or more surface fractures over the last 3500 years. In the last 2500 years time period, there are five surface fractures in the earthquakes that have occurred in this region and that the interval of earthquake recurrence has changed between 210–700 years.

Kaypak and Eyidogan (2002, 2005) have studied to determine the upper crustal velocity of Erzincan and its surroundings. When new aftershocks calculated by the seismic velocity structure are examined, they have found that they usually fall on the North Anatolian Fault Belt, but the seismic activity is directed to the south towards Pülümür. These studies reveal that there may be a new zone of weakness between the southern part of the basin and Pülümür. They have identified six layers at different seismic velocities in the Erzincan Basin, 20 km above the shell. In addition to the aftershocks of the 1992 Erzincan earthquake, the regional seismic activity after the 2003 Pülümür earthquake indicated that a new fault called the Avcıdag Fault antithetically to the North Anatolian Fault Zone similar to the Ovacık Fault developed.

Akpınar et al. (2016), paleomagnetic samples were taken from the lavas in the Quaternary volcanic outlet centers closely related to the NAFZ, especially on the northern edge of the Erzincan Basin. When paleomagnetism results of samples taken from 43 different stations in Erzincan Basin are examined, it is seen that all of the samples show a positive inclination value and thus contain a normal polarity. These results show that all of the young volcanic rocks in the Erzincan Basin are in Brunhes Chron.

Berge-Thierry (2001) simulated the 1992 Erzincan depremination with kinematic source model. They did this work for a 60 km × 60 km area, including the Erzincan Basin, and as a result they formed theoretical acceleration map. According to the results obtained from this map, especially the western part of the basin has shown that the level of strong ground movements that can occur in the future will be higher than 1992 level.

Volcano-sedimentary Guaratubinha Basin in southern Brazil was evolved in late Neoproterozoic due to collisional strike-slip tectonics. Aeromagnetic anomalies were investigated to present fault lines with similar methods in this study (Barao et al., 2017).

The aim of this study is to determine depth and geometry of the basin and extension of the buried surface fractures that may have developed during the historical period, which can not be detected any geomorphological and geologic signs in the surface of the young basin fill deposits today. Within the scope of this study, data obtained from geophysical studies were evaluated by geophysical and geological studies carried out in Erzincan Basin to date.

Erzincan Basin is modeled in three dimensions using gravity data of the study area. Thus, the deep structure of the Erzincan Basin has been determined, and derivation based boundary detection filters have been applied to the gravity data to reveal the discontinuities and geological boundaries of the region. The obtained information was compared with the existing surface geology and the compatibility between the formations was checked. In addition to the discontinuities determined from surface observations, new discontinuities were found in the light of the obtained results.

General Geology of Erzincan Basin

The Erzincan Basin is the largest of several strike-slip basins formed along the NAFZ on the pre-Pliocene basement located on the sidelines of the Eurasian plate and Anatolian plate. Pre-upper Cretaceous (Aktimur et al., 1995) or pre-Maastrichtian (Rice et al., 2009) basement is divided into two divisions comprising northern and southern blocks (Aktimur et al., 1995). The northern block includes Permo-Triassic metamorphic rocks, Liassic-Dogger volcano-sedimentary rocks and Upper Jurassic–Cretaceous limestone, marl and clay. The southern block is composed of Permian to Cretaceous limestones underlain unconformably Palaeozoic metamorphic rocks consisting of gneiss and muscovite-quartz-calc schists (Aktimur et al., 1995; Okay and Sahinturk, 1997; Rice et al., 2009) (Figure 1). Ophiolitic nappes of Lower Campanian–Lower Maastrichtian rock units are also observed in both blocks (Yılmaz, 1985; Aktimur et al., 1995; Kocuyigit et al., 2001; Rice et al., 2009).

These older units in the study area is unconformably covered by Upper Cretaceous–Early Eocene turbiditic calcarenite, sandstone, laminated mudrock, volcanoclastic sedimentary rocks that includes rare andesitic lava (Yılmaz, 1985; Aktimur et al., 1995; Kocuyigit et al., 2001; Rice et al., 2009). The youngest part of the basement is Miocene cover rocks including limestone, marls, green clay, evaporites and fluvial deposits (Tuysuz, 1993; Westaway and Arger, 2001; Kocuyigit, 2003; Rice et al., 2009) overlay pre-Eocene units.

The Erzincan Basin is filled by Plio-Quaternary sediments consisting of playa deposits, clastics and basin margin conglomerates. The conglomerates along the NW margin of the basin are composed of ophiolitic melange clastics and Cretaceous-Miocene carbonates (Barka and Gulen, 1989). The thickness of the basin infill is a controversial subject and changes from 500 to 4000 m (Irrlitz, 1972; Hempton and Dunne, 1984; Buyukasikoglu, 1992; Gaucher, 1993; Bernard et al., 1997; Aktar et al., 2004; Kaypak and Eyidogan, 2005; Gürbüz, 2010; Avsar et al., 2013) (Figure 2).

Tectonics and seismotectonics of the study area

It is known that the volcanic outcropping centers with Neogene-Quaternary age on the north side of the Erzincan Basin, which is one of the youngest sedimentary basins developed on the NAFZ which is one of the most active strike-slip fault zones in Turkey, are closely related to the NAFZ. The Erzincan Basin is different from the other basins on the NAFZ due to its long axis being NW-SE and related with young structures. The NW-SE extent of the basin is parallel to the extent of the NAFZ and the main segment of the NAFZ

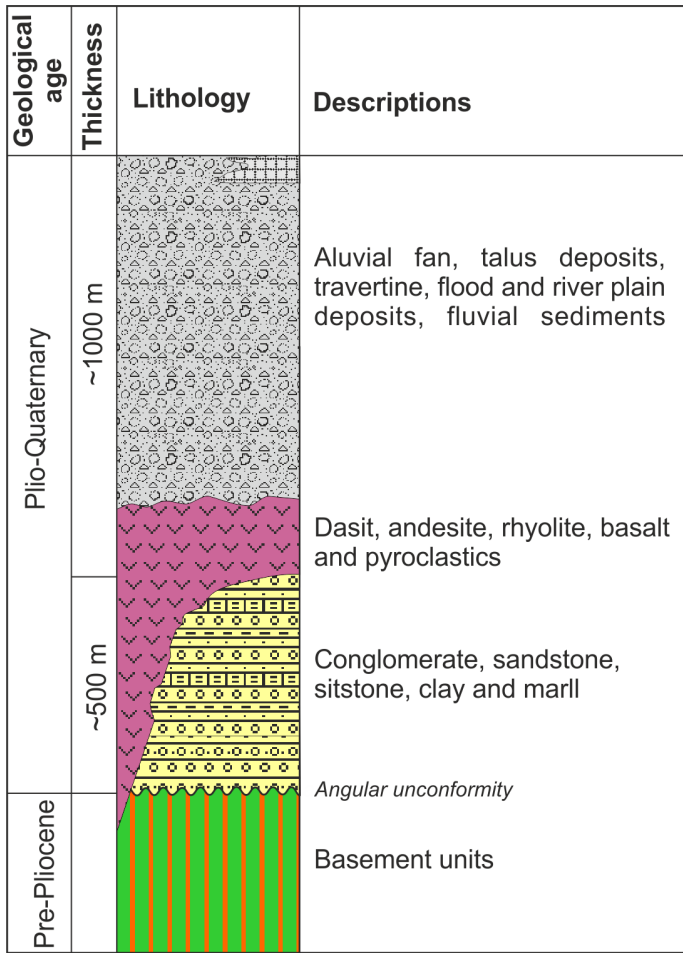


Figure 1. Generalized stratigraphic section of the study area and its vicinity (modified from Aktimur et al., 1995).

extends along the northern edge of the Erzincan Basin. The volcanic cones lined up along the northern margin present an approximate parallel to the course of this main segment. The NAFZ contains three main segments in the region (Figure 3). The location and geometry of these segments is important for understanding the origin and development of the Erzincan Basin (Akpınar, 2010).

The eastward movement of the Northeast Anatolian Block causes complex deformations for the block and the left-lateral movements in the Northeast Anatolian Fault Zone (NEAFZ), which forms the northern boundary of this block. The left-lateral strike-slip Ovacık fault intersects with the NAFZ in the southeast of Erzincan Basin. The Erzincan Basin is a NW-SE directional pull-apart type (Allen, 1969) with a length of about 50 km and a width of up to 15 km. The part of the NAFZ near Erzincan consists of many segments. The first of these segments extends from Karhova to the west of Yedisu and the second extends from the west of Yedisu to the southeast end of Erzincan Basin. The third constitutes the northeastern border of the Erzincan Basin and continues northward with a second segment. The geological and seismic properties of these fault segments are discussed in detail (Allen, 1969, Toksoz et al., 1979). The North Anatolian Fault Zone (NAFZ), Northeast Anatolian Fault Zone (NEAFZ) and Ovacık Fault (OF) form the most important tectonic structures in this area, forming a geometric conjugation with each other in the Erzincan Basin and its immediate vicinity. Most of the historical earthquakes are closely related to these three major faults movements. Earthquake distribution and topographic map of the study area are given in Figure 4.

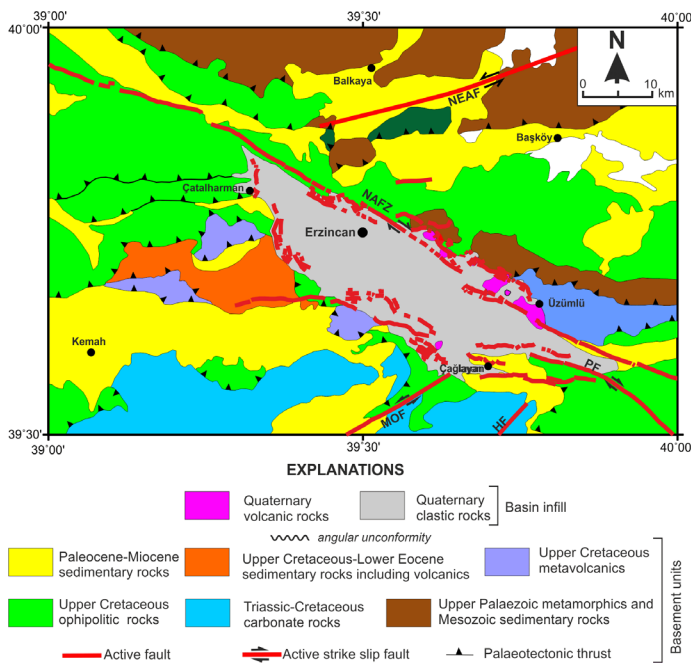


Figure 2. General geological map of Erzincan Basin and its surrounding (modified from Tarhan, 2002; Rice et al., 2009; Emre et al., 2012; Akpınar et al., 2016). HF: Heltepe Fault, NAFZ: North Anatolian Fault Zone, NEAFZ: North Eastern Anatolian Fault Zone, MOF: Malatya-Ovacık Fault, PF: Pülümür Fault.

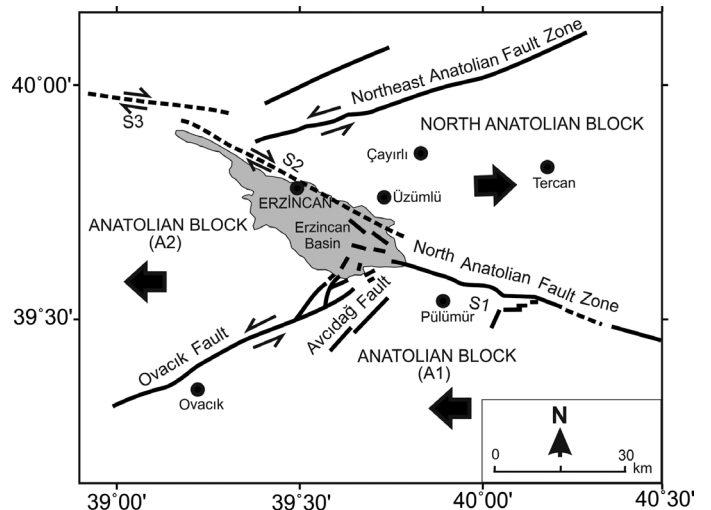


Figure 3. Tectonic blocks in Erzincan Basin and surrounding area and the direction of movement of these blocks (simplified from Barka and Gulen, 1989; Barka and Eyidoğan, 1993; Kaypak and Eyidoğan 2002). S1, S2 and S3 are the segments of the North Anatolian Fault Zone (NAFZ) (Akpınar, 2010).

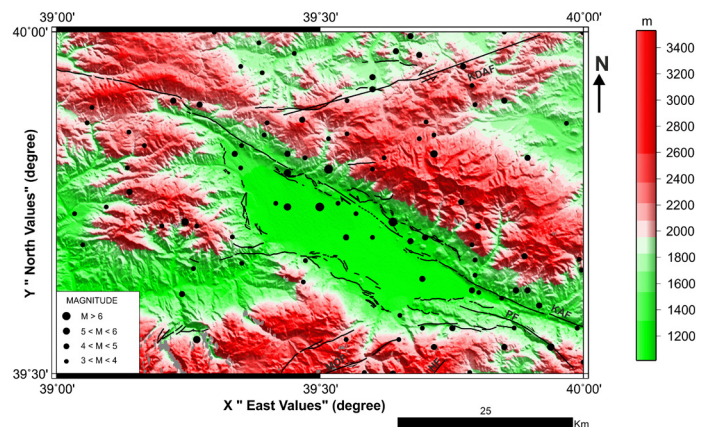


Figure 4. Earthquake distribution in study area (between 1900 and 2014) and topographic map. HF: Heltepe Fault, NAFZ: North Anatolian Fault Zone, NEAFZ: North East Anatolian Fault Zone, MOF: Malatya-Ovacık Fault, PF: Pülümür Fault.

Gravity Data and Process

Gravity data for the study area was obtained from the General Directorate of Mineral Research and Exploration (MTA) with a spacing of 2.5 km measured annually ground survey campaigns in 1970s and all corrections were made by the MTA. The density value of 2.67 gr cm^{-3} was reconstructed according to the density value of 2.40 gr cm^{-3} for the reason that the basin filling material is composed of alluvium. The gravity anomaly map of the study area is given in Figure 5.

Upward continuation

The effects of the infinite number of masses at different depths and at different points of the earth are measured as gravity anomalies on the surface. The gravity values measured from the surface are gravity anomalies originating from the densities of the masses found both on the surface and in the deep. In order to detect the anomalies originating from the masses in deep, the effect of shallow masses close to the surface must be removed, for which the "upward continuation" method has to be applied.

Potential area farther from the source at any point of the known potential area on the surface can be calculated by upward continuation method. It is necessary to measure at different heights due to various reasons, but it is desirable that these measurements be at a certain level. The values are moved to a fixed surface with the upward continuation process. Furthermore, deep anomalies due to anomalies originating from the masses in the surface may not be observed clearly. In this case, the anomalies formed by the deeper masses are brought to a more prominent position by the upward continuation process (Blakely, 1995).

The effects on the anomalies of the shallow structures were removed and the structures in the vicinity were allowed to be seen clearly by the upward continuation method in this study. Upward continuation of 0.25 km, 0.50 km, 0.75 km, 1 km, 2 km and 3 km was applied to the gravity data shown in Figure 5. It was observed that many effects were lost for 2 km and 3 km according to other continuation applications in the data. For this reason, 0.25 km, 0.50 km, 0.75 km and 1 km upward continuation were taken into consideration.

Derivative methods

The subtle details in the potential field anomaly maps can be made more visible through some derivative based filters (Ekinci and Yigitbas, 2012 and 2015, Ekinci et al. 2013). Many boundary detection filters have been proposed to determine the boundaries of potential field sources. Application of total horizontal derivatives and analytic signal filters, the first generation of boundary detection filters, is now standard. Total Horizontal Derivative (THD) filter is given by equation (1) (Cordell and Grauch, 1985).

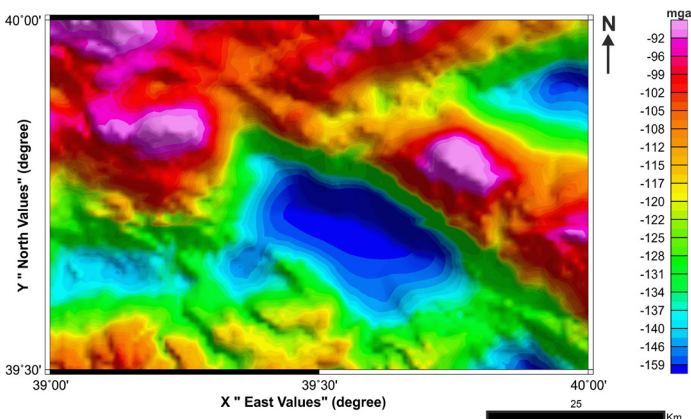


Figure 5. Gravity anomaly map for the study area

$$THD = \sqrt{\left(\frac{\partial P}{\partial x}\right)^2 + \left(\frac{\partial P}{\partial y}\right)^2} \quad (1)$$

Where, P is the gravity field, x and y are directions. The highest amplitude values of the THD output pass over the source limits. The analytical Signal (AS) amplitude is given by Nabighian (1972) for the 2B state with Eq. (2), by Roest et al. (1992) for the 3B state with Eq. (3).

$$|AS| = \sqrt{\left(\frac{\partial P}{\partial x}\right)^2 + \left(\frac{\partial P}{\partial z}\right)^2} \quad (2)$$

$$|AS| = \sqrt{\left(\frac{\partial P}{\partial x}\right)^2 + \left(\frac{\partial P}{\partial y}\right)^2 + \left(\frac{\partial P}{\partial z}\right)^2} \quad (3)$$

Where, P is the gravity field, x, y and z are directions. The AS filter is often used in potential area data collection especially for close surface exploration. The AS amplitude provides bell-shaped anomalies on the source structures. Researchers have developed filters under the heading of normalized derivative methods in recent years.

The first developed filter in this concept is the Tilt Angle (TA) filter and given by the following Eq. (4) by Miller and Singh (1994);

$$Tilt = \tan^{-1} \left(\frac{\frac{\partial P}{\partial z}}{THD} \right) \quad (4)$$

The TA is the normalized form of the vertical derivative proportional to the THD. The TA is a filter that gives the effects of both near surface and deep sources at the same amplitude level. The amplitude of the TA is positive when it is on the structure, zero when it is on the structure edge and negative values when it is outside of the structure. Amplitude values range from $-\pi/2$ to $\pi/2$ and are very easy to interpret on this. The TA is mainly a plan or shape-determining filter. For this reason, Verdusco et al. (2004) showed that the total horizontal derivative of the TA can be used to determine the boundary. Total horizontal derivation of TA is given by Eq. (5).

$$THDR = \sqrt{\left(\frac{\partial Tilt}{\partial x}\right)^2 + \left(\frac{\partial Tilt}{\partial y}\right)^2} \quad (5)$$

The total horizontal derivation of the TA causes an increase noise on data because of a derivation-based filter is calculated again. Another weakness is that it can not produce effective results against deep structures. On the other hand, the most useful feature is that it is independent of magnetization direction. For this reason, it is a filter that is often referred to in practice.

Another filter developed under the concept of normalised derivatives is Theta-Angle ($\cos \theta$) filter. Theta Angle ($\cos \theta$) filter is given by Wijns et al. (2005) with Eq. (6)

$$\cos \theta = \left(\frac{THD}{AS} \right) \quad (6)$$

Theta Angle is the normalized form of THD using the analytical signal amplitude. Theta Angle ranges from $0 < \theta < \pi/2$. For this reason, it is quite easy to interpret. The weak point of the method is that it shows scattered effects of deep structures. Another approach is the Hyperbolic Tilt Angle (HTA) filter proposed by Cooper and Cowan (2006) and is given by Eq. (7).

$$HTA = \Re \left(\tan^{-1} \left(\frac{\frac{\partial P}{\partial z}}{\sqrt{\left(\left(\frac{\partial P}{\partial x}\right)^2 + \left(\frac{\partial P}{\partial y}\right)^2\right)}} \right) \right) \quad (7)$$

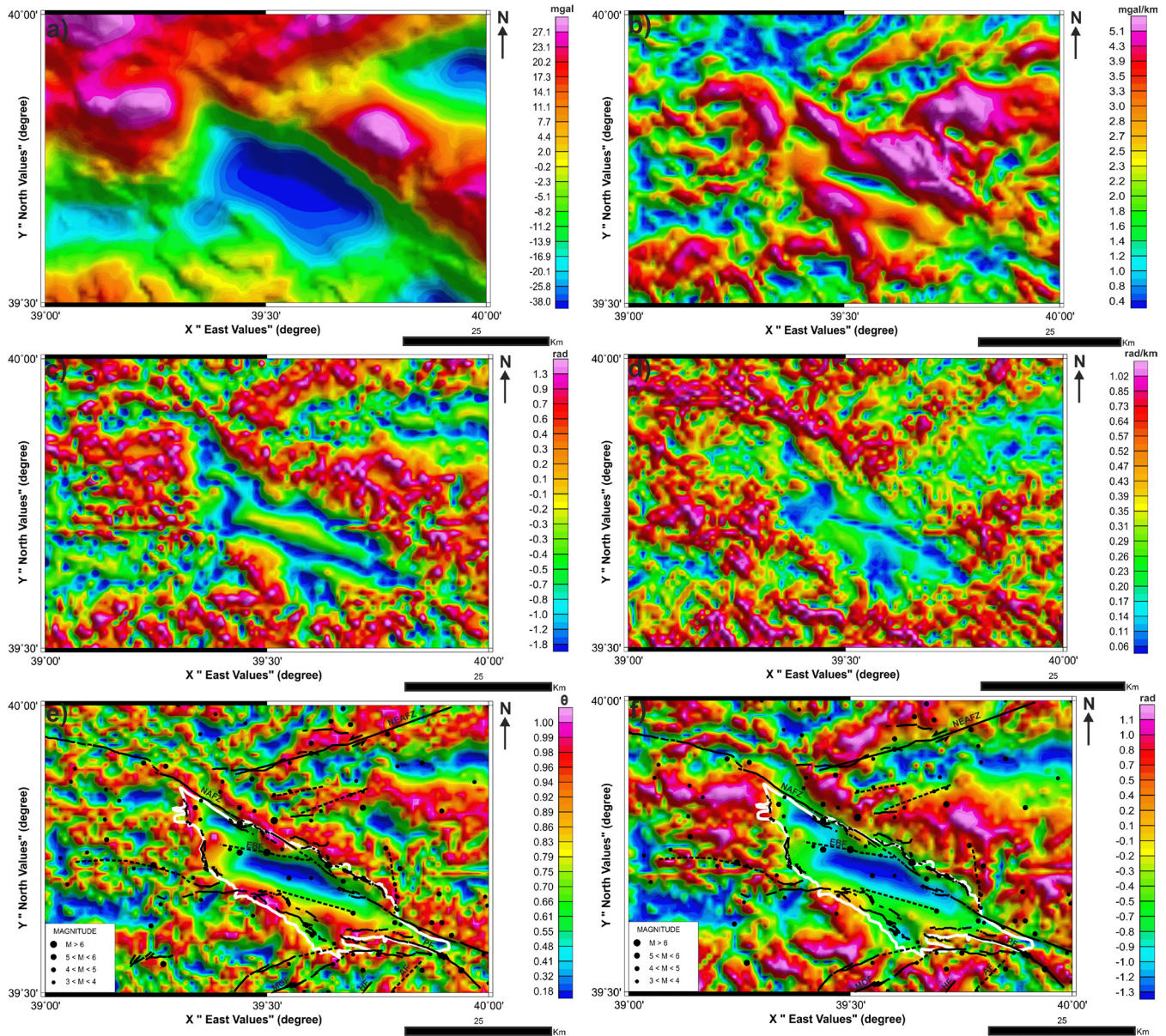


Figure 6. (a) 0.25 km upward continued gravity anomaly map (b) Application of Total Horizontal Derivative (TDH) filter applied to 0.25 km upward continued gravity data shown in Figure 6a. (c) Application of Hyperbolic Tilt Angle Derivative (HTA) filter applied to 0.25 km upward continuation applied gravity data shown in Figure 6a. (d) Application of Total Horizontal Derivative (THDR) filter of 0.25 km upward continuation applied gravity data shown in Figure 6a. (e) Application of 0.25 km upward continuation applied gravity data Theta Angle Derivative ($\cos \theta$) filter shown in Figure 6a. (f) Application of Tilt Angle Derivative (Tilt) filter Applied to 0.25 km upward continuation applied to gravity data shown in Figure 6a. AF: Avcıdagi Fault, EBF: Erzincan Basin Fault, HF: Heltepe Fault, NAFZ: North Anatolian Fault Zone, NEAFZ: North Eastern Anatolian Fault Zone, MOF: Malatya-Ovacık Fault, PF: Pülümür Fault. White line shows boundary of Erzincan Basin.

In Figure 6, five derivative filters were applied to the gravity data which was applied 0.25 km upward continuation.

Five derivative filters were applied to the gravity data which was applied 0.50 km upward continuation. The map of the gravity anomaly applied to the derivative filters is shown in Figure 7.

Five derivative filters were applied to the gravity data which was applied 0.75 km upward continuation. The map of the gravity anomaly applied to the derivative filters is shown in Figure 8.

Five derivative filters were applied to the gravity data which was applied 1.0 km upward continuation. The map of the gravity anomaly applied to the derivative filters is shown in Figure 9.

When the maps obtained as a result of the derivative methods applied for each level given in this section are examined, the derivation methods in which the structure boundary and discontinuities are observed most clearly in accordance with the purpose of the study are determined as Tilt and Theta Angles. For this

reason, the results of Tilt and Theta Angle derivation methods are compared with the existing surface faults in five different derivation methods. In addition, the discontinuities that are not seen on the surface and compatible with the existing earthquakes are shown with cut lines on Tilt and Theta Angle maps of each extension level (Figures 6e,6f, 7e,7f, 8e,8f and 9e,9f).

Three dimensional (3D) model of depth

In Cordell and Henderson's (1968) 3D modeling method, gravity anomaly is rectangularly gridded. Here, each grid point is the center of the vertical prismatic structure, and the cross-sectional dimensions of the prisms are the grid spacing. In this way the data is divided into equal prisms as grid point. The first approach model of structure is derived from the Bouguer slab relationship. The gravitational field of the first model is calculated and the ratio of the calculated gravity value with the measured value at each grid point is used to modify the

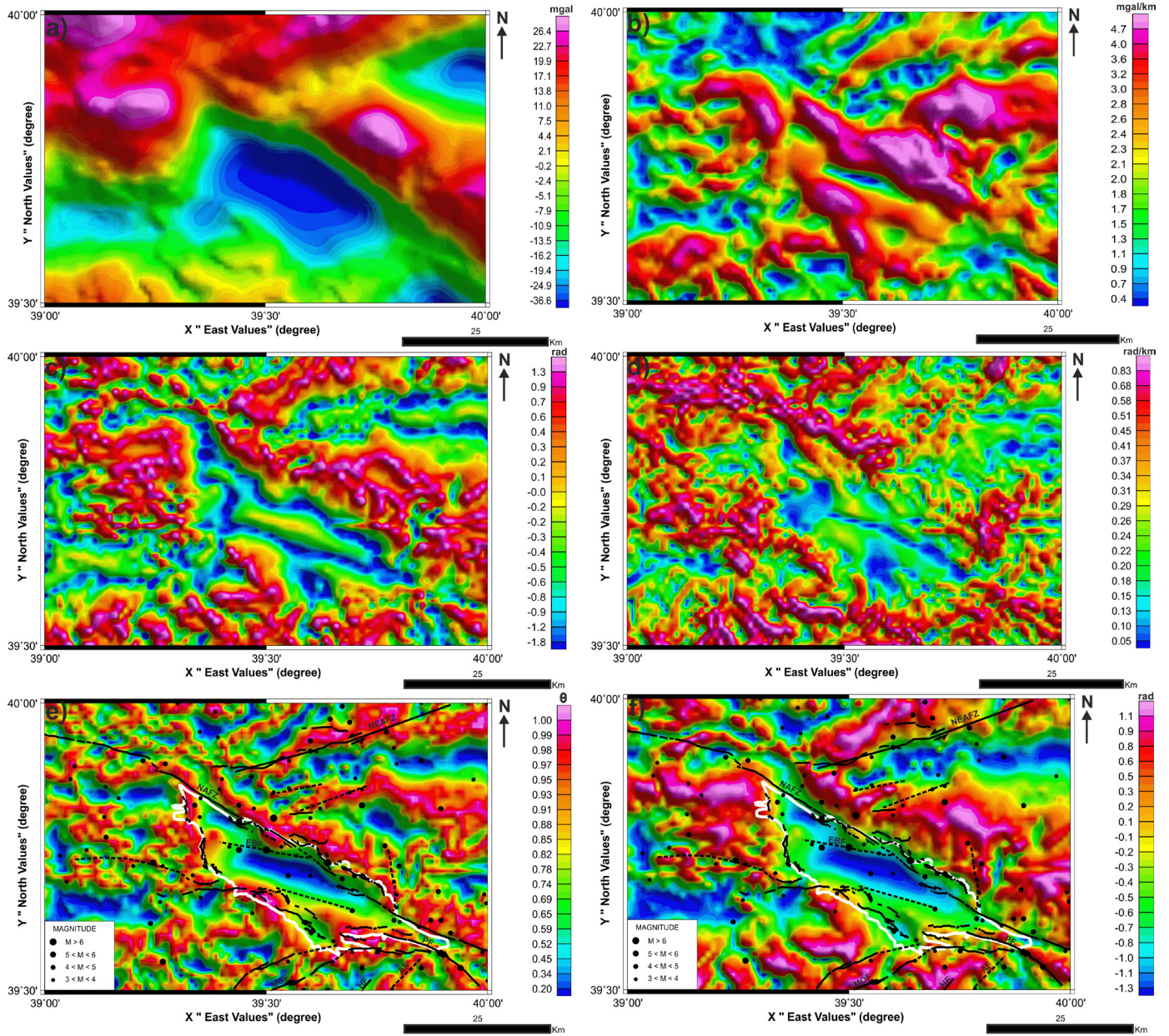


Figure 7. (a) 0.50 km upward continued gravity anomaly map. (b) Application of Total Horizontal Derivative (THD) filter applied to 0.50 km upward continued gravity data shown in Figure 7a. (c) Application of Hyperbolic Tilt Angle Derivative (HTA) filter applied to 0.50 km upward continuation applied gravity data shown in Figure 7a. (d) Application of Total Horizontal Derivative (THDR) filter of 0.50 km upward continuation applied gravity data Slope Angle shown in Figure 7a. (e) Application of 0.50 km upward continuation applied gravity data Theta Angle Derivative ($\cos \theta$) filter shown in Figure 7a. (f) Application of Tilt Angle Derivative (Tilt) filter applied to 0.50 km upward continuation applied to gravity data shown in Figure 7a. AF: Avcıdagı Fault, EBF: Erzincan Basin Fault, HF: Heltepe Fault, NAFZ: North Anatolian Fault Zone, NEAFZ: North Eastern Anatolian Fault Zone, MOF: Malatya-Ovacık Fault, PF: Pülümür Fault. White line shows boundary of Erzincan Basin.

initial structure model, thus leading to the second model of the structure. This process is repeated until the best fit between measured and calculated gravity data. In this method, the model building is assumed to be homogeneously distributed in its density and limited along a reference plane at a certain depth. Most of the iterative modeling methods consist of three steps. These

- 1) The initial model,
- 2) Calculation of the gravitational effect of the experimental model,
- 3) Modification of the model.

The second and third steps are repeated until sufficient alignment is achieved. The position of each prism element is established by a regular relationship for a specified horizontal reference surface. There are three modes for the reference surface of the prism elements. These are the upper surface, the

lower surface and the midpoint. These are the upper surface, the lower surface and the midpoint. Firstly, the density and the reference plane are specified, and the gravity effect $P(x, y, 0)$ on the vertical prism $Q(x', y', 0)$ at the q^{th} grid point is only a function of the prism thickness T_q and the corresponding position (Eq. 8).

$$\Delta g_{obs,p} \approx \gamma f(P, Q, T_q; \rho, D) \quad (8)$$

and the gravity effect of the input causal structure at the p^{th} grid point

$$g_{obs,p} \approx \sum_{q=1}^M \gamma f(P, Q, T_q; \rho, D) \quad (9)$$

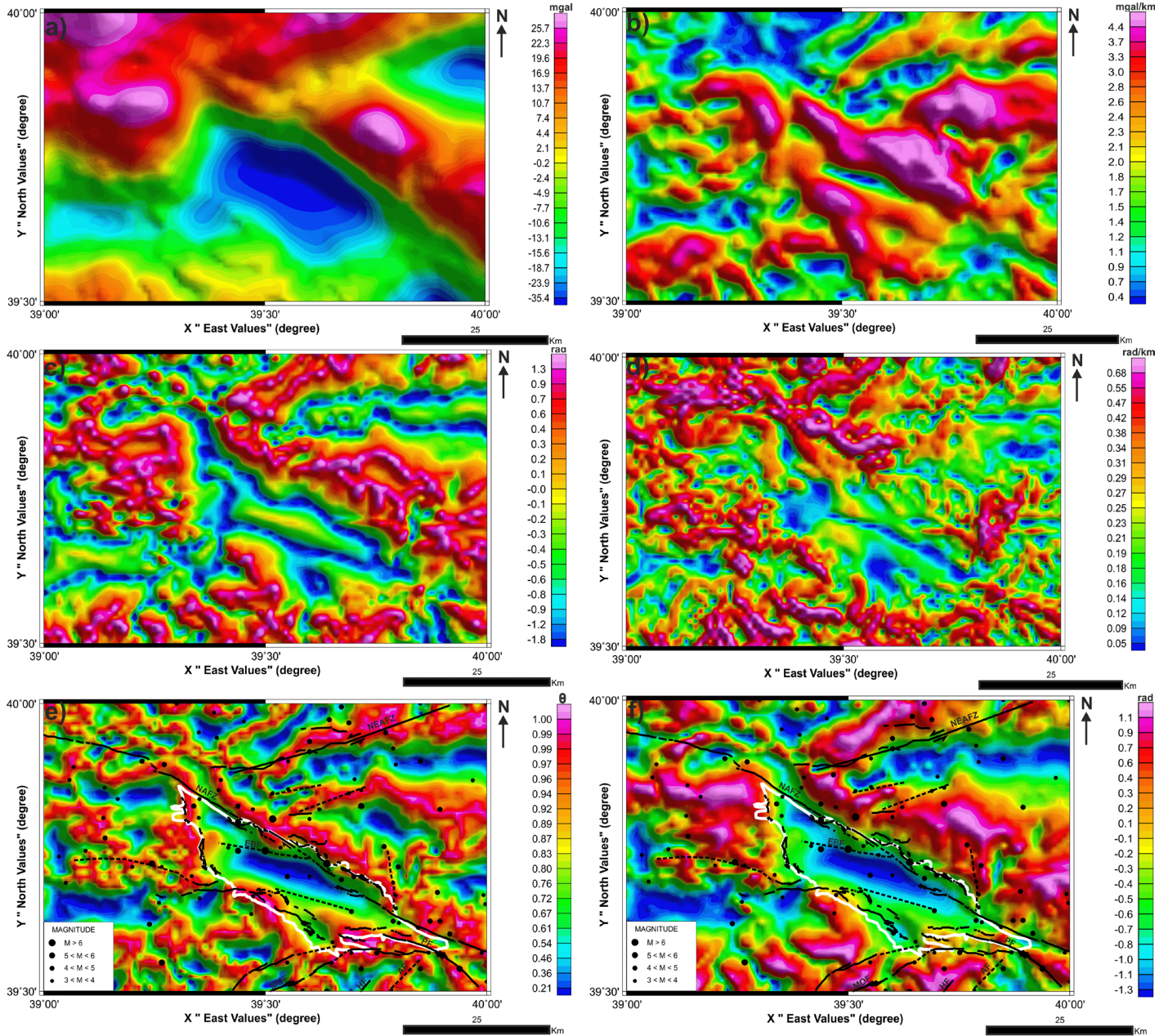


Figure 8. (a) 0.75 km upward continued gravity anomaly map. (b) Application of Total Horizontal Derivative (TDH) filter applied to 0.75 km upward continued gravity data shown in Figure 8a. (c) Application of Hyperbolic Tilt Angle Derivative (HTA) filter applied to 0.75 km upward continuation applied gravity data shown in Figure 8a. (d) Application of Total Horizontal Derivative (THDR) filter of 0.75 km upward continuation applied gravity data Slope Angle shown in Figure 8a. (e) Application of 0.75 km upward continuation applied gravity data Theta Angle Derivative ($\cos \theta$) filter shown in Figure 8a. (f) Application of Tilt Angle Derivative (Tilt) filter Applied to 0.75 km upward continuation applied to gravity data shown in Figure 8a. AF: Avcıdagı Fault, EBF: Erzincan Basin Fault, HF: Heltepe Fault, NAFZ: North Anatolian Fault Zone, NEAFZ: North Eastern Anatolian Fault Zone, MOF: Malatya-Ovacık Fault, PF: Pülümür Fault. White line shows boundary of Erzincan Basin.

expressed by Equation (9). Here
 γ = gravitational constant
 ρ = density
 D = depth of reference plane
 M = the total number of grids.

If t_n is the thickness of the prism element under the q^{th} grid point as a result of q^{th} iteration,

$$\lim_{n \rightarrow \infty} t_{n,q} = T_q \quad (10)$$

is expressed as Eq. (10). Initial model thicknesses at each grid point

$$t_{1,q} = K g_{\text{obs},q} \quad (11)$$

is expressed as Eq. (11). Here

$$K = \frac{1}{2\pi\gamma\rho}$$

Thus, the calculated gravity anomaly of the first model,

$$g_{\text{calc},1,p} = \sum_{q=1}^M \gamma f(P, Q, t_{1,q}; \rho, D) \quad (12)$$

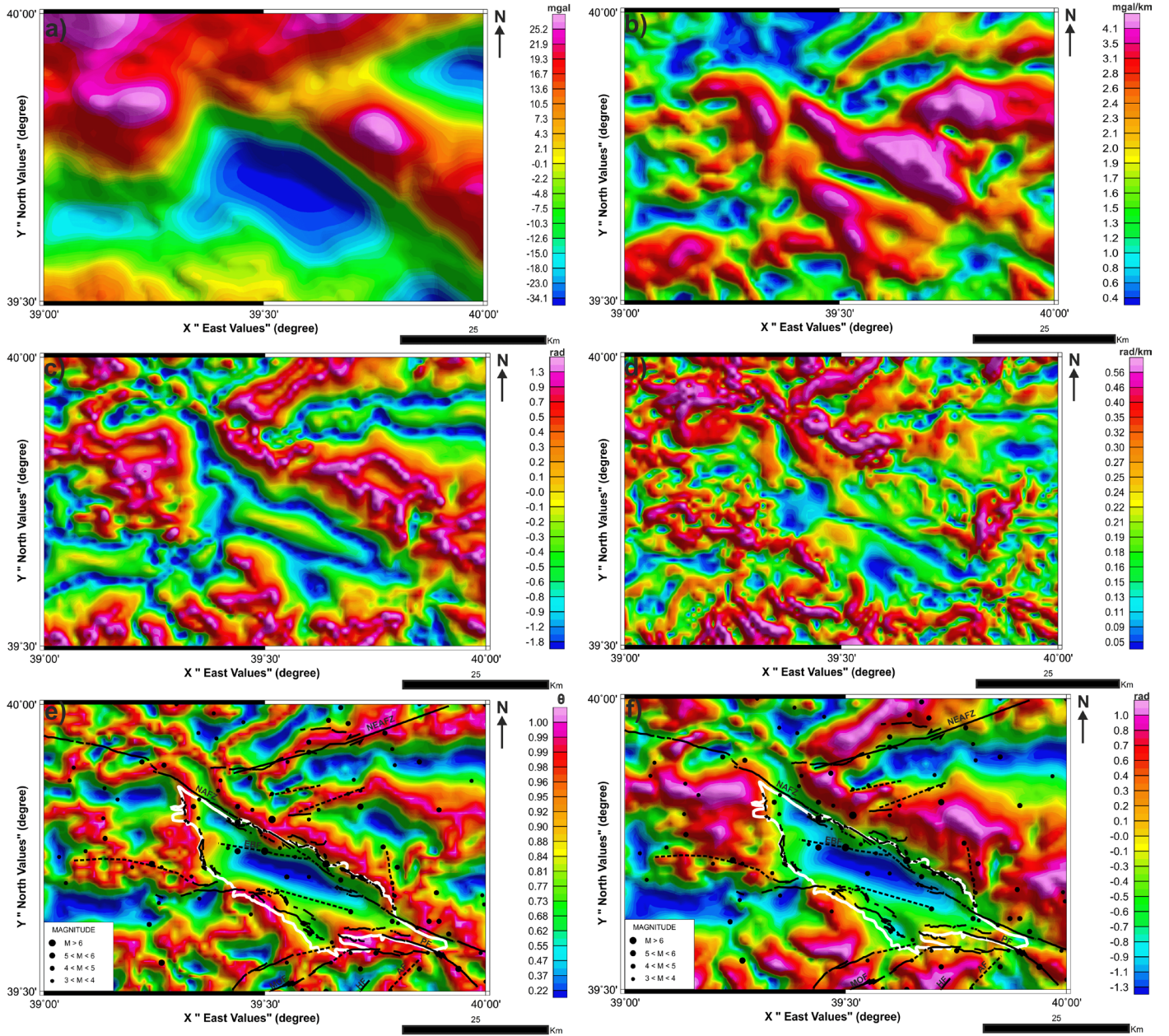


Figure 9. (a) 1.0 km upward continued gravity anomaly map. (b) Application of Total Horizontal Derivative (THD) filter applied to 1.0 km upward continued gravity data shown in Figure 9a. (c) Application of Hyperbolic Tilt Angle Derivative (HTA) filter applied to 1.0 km upward continuation applied gravity data shown in Figure 9a. (d) Application of Total Horizontal Derivative (THDR) filter of 1.0 km Upward continuation applied gravity data Slope Angle shown in Figure 9a. (e) Application of 1.0 km upward continuation applied gravity data Theta Angle Derivative ($\cos \theta$) filter shown in Figure 9a. (f) Application of Tilt Angle Derivative (Tilt) filter applied to 1.0 km upward continuation applied to gravity data shown in Figure 9a. AF: Avcıdagi Fault, EBF: Erzincan Basin Fault, HF: Heltepe Fault, NAFZ: North Anatolian Fault Zone, NEAFZ: North Eastern Anatolian Fault Zone, MOF: Malatya-Ovacık Fault, PF: Pülümür Fault. White line shows boundary of Erzincan Basin.

is expressed as Eq. (12). In the next iteration, the thickness is defined by the following equation (13).

$$t_{2,q} = t_{1,q} \left(\frac{g_{obs,q}}{g_{calc,1,q}} \right) \quad (13)$$

or in general

$$t_{n+1,q} = t_{n,q} \left(\frac{g_{obs,q}}{g_{calc,n,q}} \right) \quad (14)$$

and so

$$g_{calc,n,p} = \sum_{q=1}^M \gamma f(P, Q, t_{n,q}); \rho, D \quad (15)$$

can be written Eq. (15). The rms values are calculated to determine the fit between the measured and calculated data.

$$rms_n = \sqrt{\frac{\sum_{p=1}^M (g_{obs,p} - g_{calc,n,p})^2}{M}} \quad (16)$$

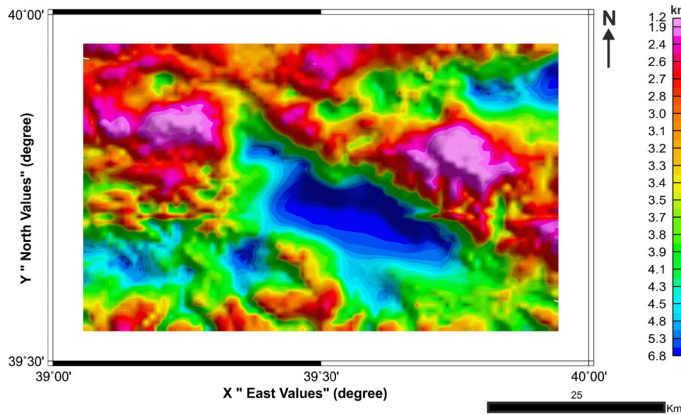


Figure 10. 3D alluvial thickness map for the study area.

Thus, the iteration step, which is the smallest value of rms, is considered as a solution.

The method developed by Cordell and Henderson (1968) to determine the change of alluvium thickness of the Erzincan Basin was applied to the gravity data shown in Figure 5. The intensity value given by Akpınar (2010) was used as the density difference value (-0.86 g cm^{-3}) when three-dimensional modeling was performed. As can be seen from the 3-D depth model shown in Figure 10, the thickness of the alluvial unit forming Erzincan Basin is determined as approximately 7 km. It is also observed that the alluvium thickness decreased in the northwest part of the basin and the basin became two parts.

Results and Discussions

When the map of the gravity anomaly of the study area is examined, it is seen that it has low gravity values ($\sim -160 \text{ mgal}$) in comparison with the construction around the alluvium unit forming the Erzincan Basin. It is compatible with the surface geology map shown in Figure 3. Upward continuation of gravity anomalies are usually based on the Poisson integral and its iteration. By using the method of domain decomposition, a local function can be used for upward continuation of gravity data. This approach decomposes the total area into small domains, and uses local functions to model the disturbing potential within each of these domains. The results of the domain decomposition approach are compared to the Poisson integral for upward continuation in a flat area. In reality, gravity data are measured on the Earth's physical surface, not on the geoid, and the geoid is not a sphere. The numerical integration of Poisson's integral is time consuming. Also, the fast Fourier method can not be directly applied, if the computation points are not at the same altitude. In order to avoid large topographic effect in the Erzincan Basin, the upward continuation method was applied to the gravity data shown in Figure 6 for 0.25, 0.50, 0.75, and 1 km continuation levels. When the upward continuation map of each level is examined, it has been observed that near 2 km and 3 km upward continuation have been lost in the applied data. Therefore, 0.25, 0.50, 0.75 and 1 km upward continued gravite anomalies have been considered.

In order to determine the structure boundaries and discontinuities in the study area, five derivative filters were applied; Total Horizontal Derivative (THD) filter, Tilt Angle Derivative (Tilt) filter, Total Horizontal Derivative (THDR) filter; Angle Derivative ($\cos \Theta$) and Hyperbolic Tilt Angle Derivative Filter (HTA). When all the maps shown in Figures 6 to 9 are examined, it has been determined that the boundary of the structure and the derivative methods in which the discontinuities are observed most clearly are the Tilt and Theta Angles. For this reason, the results of the Theta Angle derivative method applied to each level of upward continuation (0.25, 0.50, 0.75 and 1 km, respectively) shown in Figures 6e, 7e, 8e, 9e were compared with the current discontinuities in the study area. When all the maps are examined, it has a value of $+1 (\pi/2)$ (pink color) on the amplitude of the Theta

Angle and is consistent with the Theta Angle values of the discontinuities shown by continuous black lines (AF, MOF, HF, NAFZ, NEAFZ and PF). The discontinuities indicated by the black lines are discontinuities determined within the scope of this study, taking into account that the values of $+1 (\pi/2)$ (pink color) in the Theta Angle maps are in line with the distribution of the existing earthquake epicenters. Furthermore, it is seen that in the northwestern part of Erzincan Basin in the Theta Angle maps, the basin is deformed and therefore two parts. In this part of the basin, it is seen that this deformation is consistent with the direction of earthquakes. For this reason, a new discontinuity is defined as EBF (Erzincan Basin Fault) in this part of the basin.

The results of Tilt and Theta Angle derivative methods are compared with the existing surface faults in five different derivation methods. The results of the Tilt Angle derivation method were applied to each of the continuation levels (0.25, 0.50, 0.75 and 1 km respectively) shown in Figures 6f, 7f, 8f, 9f were compared with the current discontinuities in the study area. When all the maps are examined, the amplitude of Tilt Angle is as $+1.5 (\pi/2)$ (pink color) on body and as 0 on edge of body. The discontinuities (AF, MOF, HF, NAFZ, NEAFZ and PF) are shown with continuous black lines are correlated with Tilt Angle amplitude. It is in line with the values of the angle. The discontinuities indicated by the dashed black lines are the discontinuities determined within the scope of this study, taking into consideration that the values of $+1 (\pi/2)$ (pink color) and 0 (yellow color) in the Tilt Angle maps are compatible with the existing earthquakes. Furthermore, in the Tilt Angle maps it is seen that in the northwest part of the Erzincan Basin there are two parts, which are not a whole as contemplated to date. In this part of the basin, it is seen that the earthquake epicenter distribution agrees with this deformation direction. For this reason, a new discontinuity is defined as EBF (Erzincan Basin Fault) in this part of the basin.

Some of the discontinuities obtained from the Tilt and Theta Angle maps are consistent with the discontinuities (continuous black lines) determined by Akpınar (2010). In this study, in addition to the results of Akpınar (2010), new discontinuities which are not seen from the surface shown by cut black lines have been determined. As a result of 3 dimensional gravity model, the thickness of the alluvial unit forming Erzincan Basin is determined as 7 km. It is also observed that the alluvium thickness decreased in the northwest part of the basin and the basin became two parts. This situation is consistent with the situation in the Tilt and Theta Angle maps. Akpınar (2010) determined the depth of the basin to be about 7.5 km from the two-dimensional gravity models formed from the gravity profiles taken perpendicular to the basin extension, and both study results are compatible with each other.

Conclusions

In this study, the extensions of the surface fractures developed in the young basin fillets of the Erzincan Basin, which can not be detected any morphological and geologic signs on the surface today, especially during the historical earthquakes, were determined by using the potential field data and the information about the three dimensional geometry of the basin. Erzincan Basin is modeled in three dimensions using gravity data of the study area. Thus, the deep structure of the Erzincan Basin has been determined, and derivation based boundary detection filters have been applied to the gravity data to reveal the discontinuities and geological boundaries of the region. The obtained information was compared with the existing surface geology and the compatibility between the formations was checked. In addition to the discontinuities determined from surface observations, new discontinuities were found in the light of the obtained results. The obtained results show that there are other extensions of the active North Anatolian Fault Zone inside and around the basin, which can not be observed on the surface today, and new data on earthquake hazard of Erzincan urban settlement area are obtained. These data have to be taken into account when working in the region. It is expected that new information and findings that will be detected in this region bearing a great earthquake risk will contribute to reducing the loss of life and property that may occur in future earthquakes.

References

- Akpınar, Z. (2010). *Erzincan Havzasının tektonik gelişiminin paleomanyetik ve potansiyel alan verileri ile incelenmesi*. PhD Thesis, Cumhuriyet University of Sivas 196 p. (In Turkish).
- Akpınar, Z., Gürsoy, H., Tatar, O., Büyüksaraç, A., Koçbulut, F. & Piper, J.D.A. (2016). Geophysical analysis of fault geometry and volcanic activity in the Erzincan Basin, Central Turkey: Complex evolution of a mature pull-apart basin. *Journal of Asian Earth Sciences*, 116, 97-114.
- Aktar, M., Dorbath, C. & Arpat, E. (2004). The seismic velocity and fault structure of the Erzincan Basin, Turkey, using local earthquake tomography. *Geophysical Journal International*, 156, 497-505.
- Aktimur, H.T., Sarıaslan, M., Kecer, M., Tursucu, A., Olcer, S., Yurdakul, M.E., Mutlu, G., Aktimur, S. & Yıldırım, T. (1995). *Erzincan Dolayının Jeolojisi [Geology of Erzincan Surrounding]*. Mineral Research and Exploration Institute (MTA) of Turkey Report no. 9792 [unpublished, in Turkish].
- Allen, C. R. (1969). *Active Faulting in Northern Turkey*, Contribution No. 1577, Div. Geol. Sci., Calif. Inst. Tech., p. 32
- Avsar, U., Turkoglu, E., Unsworth, M., Caglar, I. & Kaypak, B. (2013). Geophysical images of the North Anatolian Fault Zone in the Erzincan Basin, Eastern Turkey, and their tectonic implications. *Pure and Applied Geophysics*, 170 (3), 409-431.
- Barao L. M., Trzaskos B., Vesely F.F., de Castro L.G., Ferreira F. J.F., Vasconcellos E. M.G. & Barbosa T.C. (2017). The role of post-collisional strike-slip tectonics in the geological evolution of the late Neoproterozoic volcano-sedimentary Guaratubinha Basin, southern Brazil. *Journal of South American Earth Sciences*, 80, 29-46
- Barka, A. & Kadinsky-Cade, K. (1988). Strike-slip faulting geometry in Turkey and its influence on earthquake activity. *Tectonics*, 7, 663-684.
- Barka, A. & Gülen, L. (1989). Complex Evolution of the Erzincan Basin (Eastern Turkey) and its Pull-apart and Continental Escape Origin. *Journal of Structural Geology*, 11, 275-283.
- Barka, A. & Eyidoğan, H. (1993). The Erzincan earthquake of 13 March 1992 in Eastern Turkey. *Terra Nova*, 5, 190-194.
- Berge-Thierry, C., Bernard, P. & Herrero, A. (2001). Simulating strong ground motion with the 'k⁻²' kinematic source model: An application to the seismic hazard in the Erzincan Basin, Turkey. *Journal of Seismology*, 5, 85-101.
- Bayrak, Y., Yılmazturk, A. & Ozturk, S. (2005). Relationship between fundamental seismic hazard parameters for the different source regions in Turkey. *Natural Hazards*, 36, 445-462.
- Bernard, P., Gariel, J.C. & Dorbath, L. (1997). Fault location and rupture kinematics of the magnitude 6.8, 1992 Erzincan earthquake, Turkey, from strong ground motion and regional records. *Bulletin of Seismological Society of America*, 87, 1230-1243.
- Blakely, R.J. (1995). *Potential theory in gravity and magnetic applications*. Cambridge Press., 441 p.
- Buyukasikoglu, S. (1992). Erzincan'ın yeraltı yapısı, yerbilimci gözüyle erzincan depremi, dünü bugünü yarını ve Türkiye Deprem Sorunu. Istanbul Technical University, Istanbul, 15 December, 43-51 (in Turkish).
- Cordell, L. & Henderson, R.G. (1968). Iterative three-dimensional solution of gravity anomaly data using a digital computer. *Geophysics*, 33, 596-601.
- Cordell, L.E. & Grauch, V.J.S. (1985). *Mapping basement magnetization zones from aeromagnetic data in the San Juan Basin, New Mexico*. In: W.J. Hinze, Editor, The Utility of Regional Gravity and Magnetic Anomaly Maps, Society of Exploration Geophysicists, 181-197.
- Cooper, G.R.J. & Cowan, D.R. (2006). Enhancing potential field data using filters based on the local phase. *Computers & Geosciences*. 32(10), 1585-1591.
- Ekinci, Y.L. & Yigitbas, E. (2012). A Geophysical Approach to the Igneous Rocks in the Biga Peninsula (NW Turkey) Based on Airborne Magnetic Anomalies: Geological Implications. *Geodinamica Acta*, 25 (3-4), 267-285.
- Ekinci, Y.L., Ertekin, C., & Yiğitbaş, E. (2013). On The Effectiveness of Directional Derivative Based Filters on Gravity Anomalies for Source Edge Approximation: Synthetic Simulations and a Case Study from the Aegean Graben System (Western Anatolia, Turkey). *Journal of Geophysics and Engineering*, 10 (3), 035005.
- Ekinci, Y.L. & Yigitbas, E. (2015). Interpretation of Gravity Anomalies to Delineate Some Structural Features of Biga and Gelibolu peninsulas, and their Surroundings (north-west Turkey). *Geodinamica Acta*, 27 (4), 300-319.
- Emre, O., Duman, T.Y., Kondo, H. Olgun, S., Ozalp, S., Elmacı, H. (2012). *1:1250.000 Scale Active Fault Map Series of Turkey, Erzincan (NJ 37-3) Quadrangle*. Serial Number: 44, General Directorate of Mineral Research and Exploration (MTA), Ankara-Turkey.
- Erdik, M., Yuzugullu, O., Yılmaz, C. & Akkas, N. (1992). 13 March (Ms = 6.8) Erzincan Earthquake: A preliminary reconnaissance report. *Soil Dynamics of Earthquake Engineering*, 11, 279-310.
- Fuenzalida, H., Dorbath, L., Cisternas, A., Eyidoğan, H., Barka, A., Rivera, L., Haessler, H. & Lyberis, N. (1997). Mechanism of the 1992 Erzincan earthquake and its aftershocks, tectonics of the Erzincan Basin and decoupling on the North Anatolian Fault. *Geophysical Journal International*, 129, 1-28.
- Gaucher, E. (1993). *Modele en profondeur et en vitesse du Basin d'Erzincan*. DEA Rep. 2, Institut de Physique du Globe de Paris, Jussieu, 215-460.
- Gencoglu, S., Inan, E. & Guler, H., 1990. *Türkiye'nin Deprem Tehlikesi*, TMMOB Jeofizik Mühendisleri Odası, Ankara (In Turkish).
- Gökalp, H. (2007). Local earthquake tomography of the Erzincan Basin and surrounding area in Turkey. *Annals of Geophysics*, 50(6).
- Gündoğdu, O., Altınok, Y., Hisarlı, M. & Beyaz, H. (1992). *13 Mart 1992 Erzincan depremi gözlem değerlendirmeleri, Erzincan Depremi ve Türkiye Deprem Sorunu*, ITU, Maden Fakültesi Yayını, 56-62 (In Turkish).
- Gürbüz, A. (2010). Geometric characteristics of pull-apart basins. *Lithosphere* 2(3), 199-206.
- Hartleb, R.D., Dolan, J.F., Kozacı, O., Akyuz, S. & Seitz, G.G. (2006). A 2500-yr- long paleoseismological record of large, infrequent earthquakes on the North Anatolian Fault at Cukurcimen, Turkey. *GSA Bulletin*, 118(7/8), 823-840.
- Hempton, M.R. & Dunne, L.A. (1984). Sedimentation in Pullapart Basins: Active Examples in Eastern Turkey. *Journal of Geology*, 92, 513-530.
- Irritz, W. (1972). *Lithostratigraphie und tektonische Entwicklung des Neogens in ordostanatolien*. Beih. geol. Jb., 120(10), 1-111.
- Kaypak, B. & Eyidoğan, H. (2002). *3-D models of Vp and Vp/Vs from local earthquake tomography in Erzincan Basin, eastern Turkey*. Paper given at the *Tectonics of Eastern Turkey and the Northern Arabian Plate*. International Workshop, 23-25 Sept. 2002, Erzurum, Turkey.
- Kaypak, B. & Eyidoğan, H. (2005). One-dimensional crustal structure of the Erzincan Basin, eastern Turkey and relocations of the 1992 Erzincan earthquake (Ms = 6.8) aftershock sequence. *Physical Earth Planetary Science*, 151, 1- 20.
- Kaypak, B. (2008). Three-dimensional Vp and Vp/Vs structure of the upper crust in the Erzincan Basin (eastern Turkey). *Journal of Geophysical Research*, 113, B07307.
- Kocyyigit, A., Yılmaz, A., Adamia, S. & Kuloshvili, S. (2001). Neotectonics of East Anatolian Plateau (Turkey) and Lesser Caucasus: implication for transition from thrusting to strike-slip faulting. *Geodinamica Acta*, 14, 177-195.

- Kocyigit, A. (2003). *Two stage Evolutionary Model for the Erzincan pull-apart Basin on the North Anatolian Fault System (NAFS), Turkey. International Workshop on the North Anatolian, East Anatolian and Deadsea Fault Systems: Recent Progress in Tectonics and Paleoseismology* 31 August to 12 September, METU-Ankara, 184 (Abstract).
- Miller, H.G. & Singh, V. (1994). Potential field tilt—a new concept for location of potential filed sources. *Journal of Applied Geophysics*, 32, 213-217.
- Nabighian, M.N. (1972). The analytic signal of two-dimensional magnetic bodies with polygonal cross-section: its properties and used for automated anomaly interpretation. *Geophysics*, 37, 507-517.
- Okay, A.I. & Şahinturk, O. (1997). Geology of the Eastern Pontides, in A.G. Robinson, ed., *Regional and Petroleum Geology of the Black Sea and Surrounding Region. AAPG Memoir*, 68, 291–311.
- Pinar, A., Honkura, Y. & Kikuchi, M. (1994). Rupture process of the 1992 Erzincan earthquake and its implication for seismotectonics in eastern Turkey. *Geophysical Research Letters*, 21, 1971–1974.
- Rice, S.P., Robertson, A. H. F., Ustaomer, T., Inan, N. & Taslı, K. (2009). Late Cretaceous –Early Eocene tectonic development of the Tethyan suture zone in the Erzincan area, Eastern Pontides, Turkey. *Geological Magazine*, 146 (4), 567–590.
- Roest, W.R., Verhoef, J. & Pilkington, M., 1992. Magnetic interpretation using the 3-D analytic signal. *Geophysics*, 57(1), 116-125.
- Tarhan, N. (2002). *Türkiye Jeoloji Haritası (1:500000 ölçekli Erzurum Paftası)*, MTA Genel Müdürlüğü, Ankara (In Turkish).
- Toksöz, M.N., Şakal, A.F. and Michael, A. J., 1979. Space-time migration of earthquakes along the North Anatolian Fault Zone and seismic gaps, *Pageoph* 117, 1258–1270.
- Tüysüz, O. (1993). *Erzincan çevresinin jeolojisi ve tektonik evrimi*. In: 2nd National Earthquake Engineering Conference, Union of Chambers of Turkish Engineers and Architects Chambers of Civil Engineers, Earthquake Engineering, Turkey National Committee, Istanbul Technical University, Structural and Earthquake Research Center, 271–280 (in Turkish).
- Verduzco, B., Fairhead, J.D., Green, C.M. & MacKenzie, C. (2004). New insights into magnetic derivatives for structural mapping. *The Leading Edge*, 23(2), 116-119.
- Westaway, R.W.C. & Arger, J. (2001). Kinematics of the Malatya-Ovacik fault zone. *Geodinamica Acta*, 14, 103–131.
- Wijns, C., Perez, C. & Kowalczyk, P. (2005). Theta map: edge detection in agnetic data. *Geophysics*, 70(4), L39-L43.
- Yılmaz, A. (1985). Yukarı Kelkit Çayı ile Munzur Dağları arasının temel jeoloji özellikleri ve yapısal evrimi. *T.J.K. Bulteni*, 28(2), 79/92 (In Turkish).